Electronic Supplementary Material (ESI) for Journal of Materials Chemistry C.

Supporting Information

Generalized Seeded Growth of Ag-based Metal Chalcogenide Nanorods via Controlled Chalcogenization of the Seeds

Shutang Chen[†], Sravan Thota[†], Gabriella Reggiano[†], Jing Zhao[*,†,‡]

[†]Department of Chemistry, University of Connecticut, 55 North Eagleville Road, Storrs, Connecticut 06269-3060, United States

[‡]Institute of Materials Science, University of Connecticut, Storrs, Connecticut 06269-3136, United States

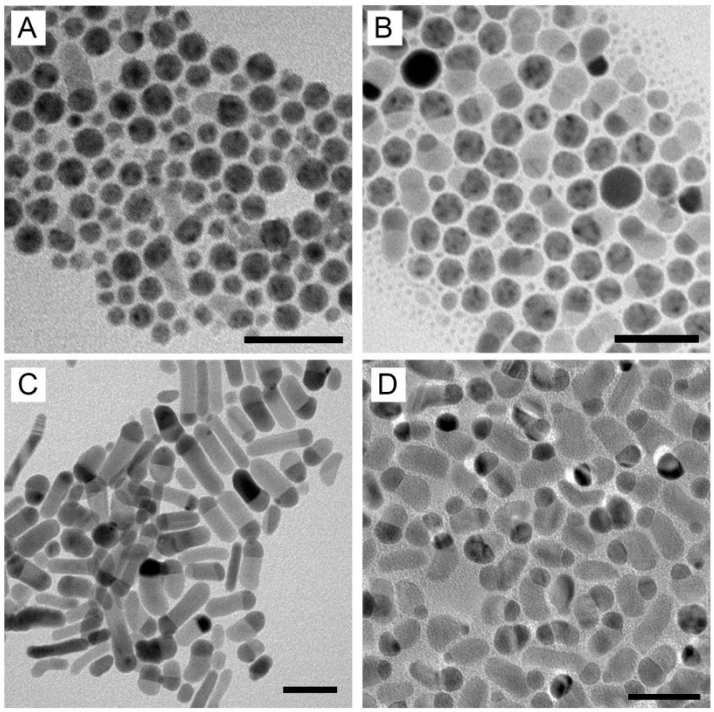

Figure S1. TEM images of Ag based hybrid nanoparticles synthesized using different sulfur precursors (A) C_8H_{17}-SH, (B) TOP + S, (C) ODE + S, and (D) OLA + S. Scale bar = 20 nm. The TEM images showed free Ag seeds existed in reaction by using C_8H_{17}-SH and trioctylphosphine sulfide as sulfur resource; whereas no free Ag seeds were found when using (ODE + S) and (OLA + S) as sulfur source.

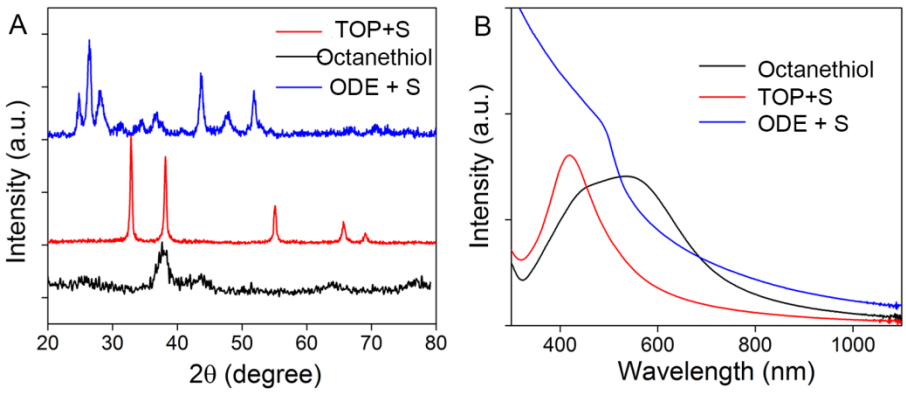

Figure S2. XRD patterns and UV-Vis spectra of Ag based hybrid nanoparticles synthesized using different sulfur precursors (A) C_8H_{17}-SH, (B) TOP + S, and (C) ODE + S. As shown in Figure S2A, no CdS or very small amount of CdS were formed by using trioctylphosphine sulfide and octanethiol as sulfur sources; while CdS and Ag_2S phase were evident when using (ODE + S) as sulfur source. XRD data results showed it was difficult to quickly release sulfur source from octanethiol and trioctylphosphine sulfide at 150 °C, owing to the strong carbon-sulfur or phosphorus-sulfur bonds. For the case of ODE + S, H_2S was produced when elemental sulfur was reduced by octadecene. The Ag seeds were easily sulfurized by the active sulfur source of H_2S. The changes in the UV-Vis spectra were consistent with composition change.

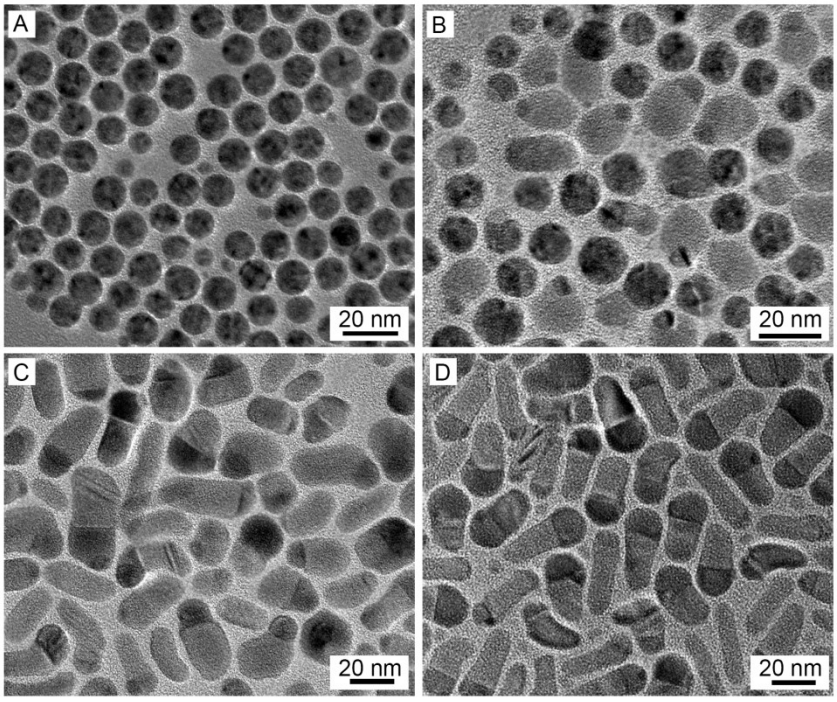

Figure S3. TEM images of Ag seeds (A), and Ag-based hybrid nanostructures prepared by injecting sulfur and cadmium precursors with different molar ratios of S/Cd, (B) S/Cd=0.5, (C) S/Cd=1.2, and (D) S/Cd=2.0.

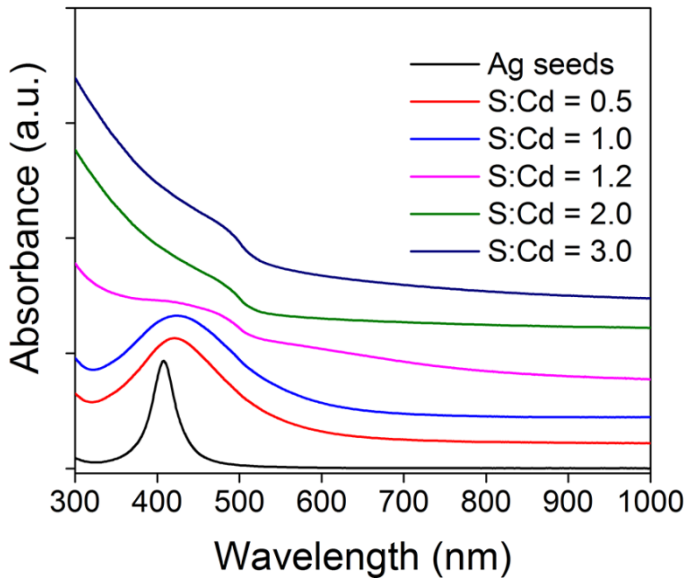

Figure S4. UV-Vis spectra of Ag seeds, and Ag-based hybrid nanostructures prepared by injecting sulfur and cadmium precursors with different molar ratios of S/Cd. Comparing the spectra in Figure S4, the absorption peaks of Ag_2S-CdS are red-shifted to 486 nm from 412 nm after complete sulfurization of the Ag seeds.

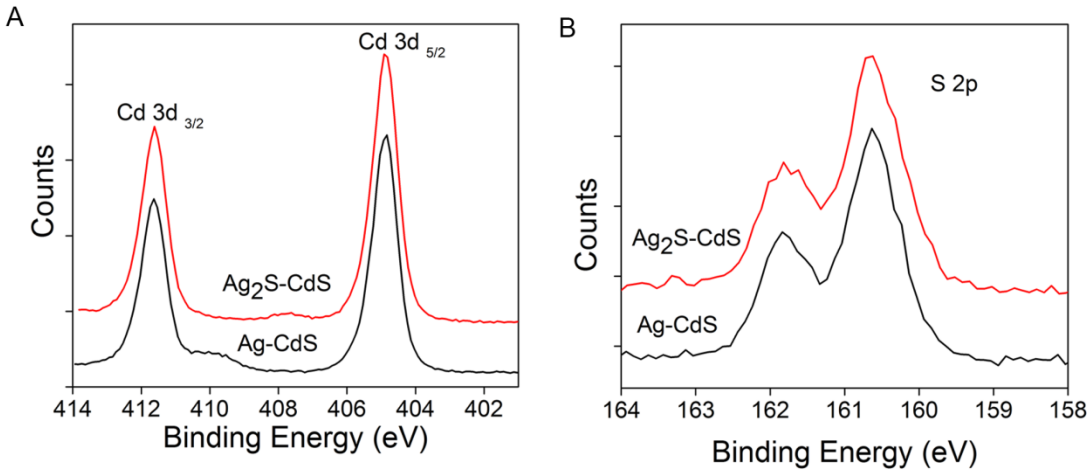

Figure S5. XPS spectra of Cd 3d (A) and S 2p for the as-prepared Ag-CdS and Ag_2S-CdS nanorods.

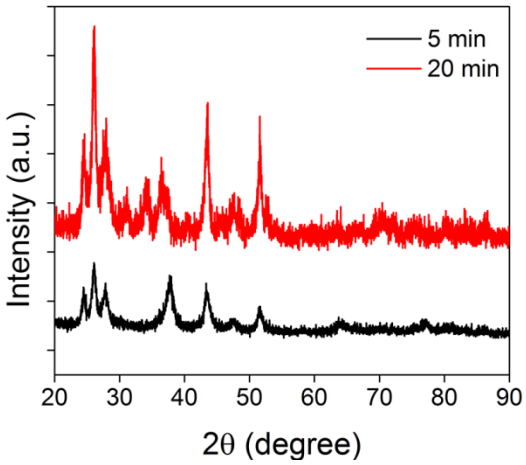

Figure S6. XRD patterns of Ag-based hybrid nanostructures prepared with S/Cd = 1 at different reaction times. XRD data indicated the Ag seeds were also easily sulfurized with the reaction time prolonging.

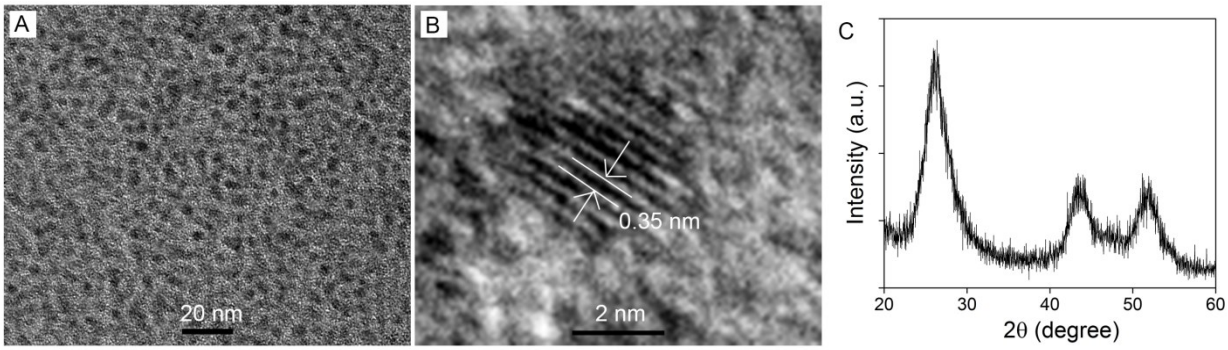

Figure S7. (A) and (B): TEM and HRTEM images of 3.0 nm CdS nanoparticles prepared without Ag seeds, and (C) the corresponding XRD pattern with cubic CdS phase. The lattice image as shown in Figure S7B reveals the growth of CdS along the (111) plane of the zinc blende structure of CdS. In the XRD pattern of spherical CdS nanoparticles, (111), (220), and (311) were indexed as CdS zinc blende phase.

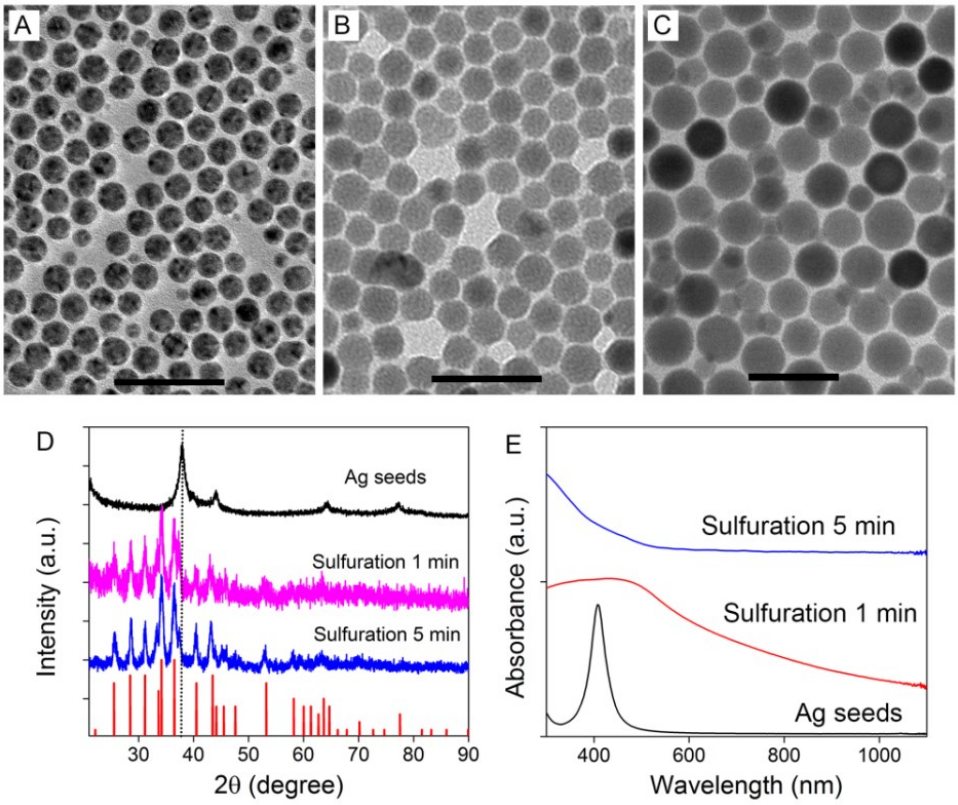

Figure S8. TEM images of Ag seeds (A), and Ag_2S nanoparticles prepared by different sulfurization time (B) 1 min, and (C) 5 min; their corresponding XRD patterns (D) and (E) UV-Vis spectra. Scale bar = 50 nm. TEM images showed the particles size increased with sulfurization time increasing. XRD data indicated sulfurization process occurred fast in our reaction within no more than 1 minute. The peak and shape of UV-Vis spectra were distinctly different after sulfurization of the Ag seeds.

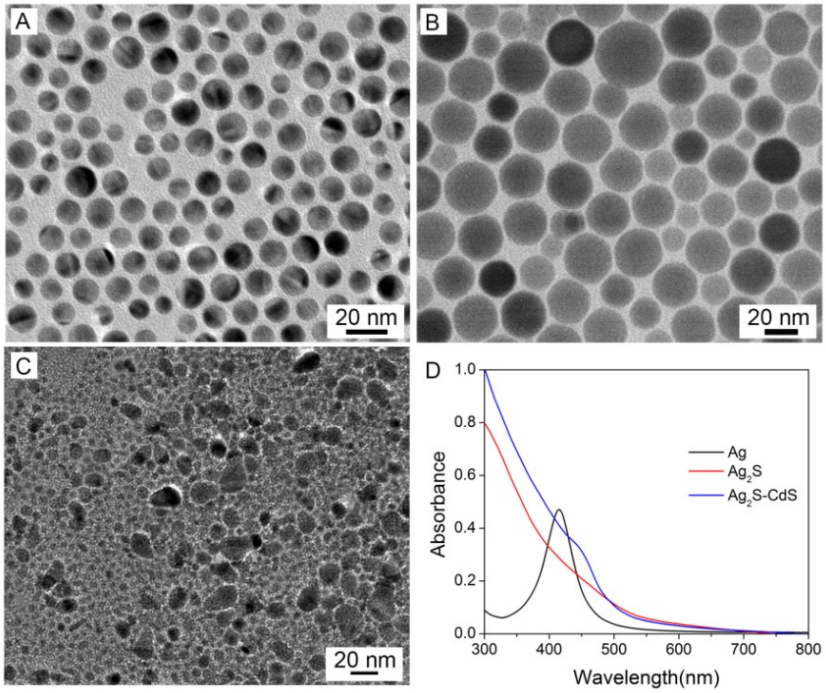

Figure S9. TEM images of (A) Ag seeds, (B) Ag_2S seeds prepared by sulfurizing Ag seeds for 5 min, (C) Ag based hybrid nanoparticles by using Ag_2S seeds, and (D) their corresponding UV-Vis spectra.

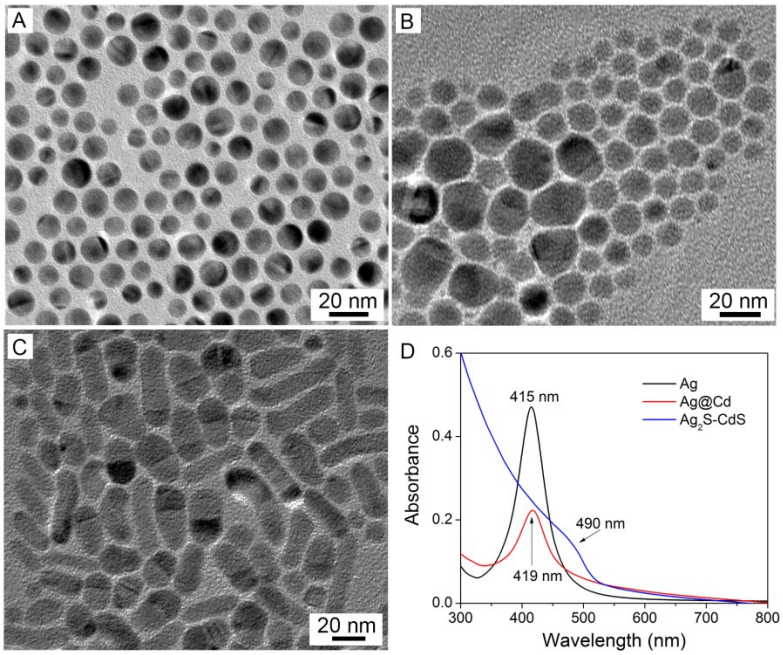

Figure S10. TEM images of (A) Ag seeds, (B) Ag-Cd seeds prepared by reduction of Cd precursor on Ag seeds for 5 min, (C) Ag based hybrid nanorods synthesized by using Ag-Cd seeds, and (D) their corresponding UV-Vis spectra.

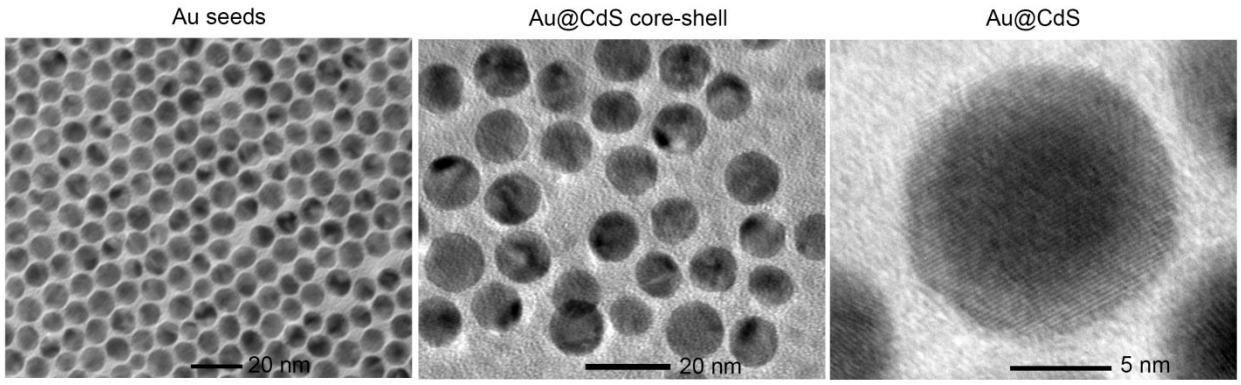

Figure S11. TEM images of Au nanoparticles and Au@CdS core-shell nanoparticles, and HETRM images of Au@CdS core-shell nanostructures. The same reaction scale and conditions were employed as described in the Ag based-CdS reactions. The only difference was that Au seeds were used instead of Ag seeds.

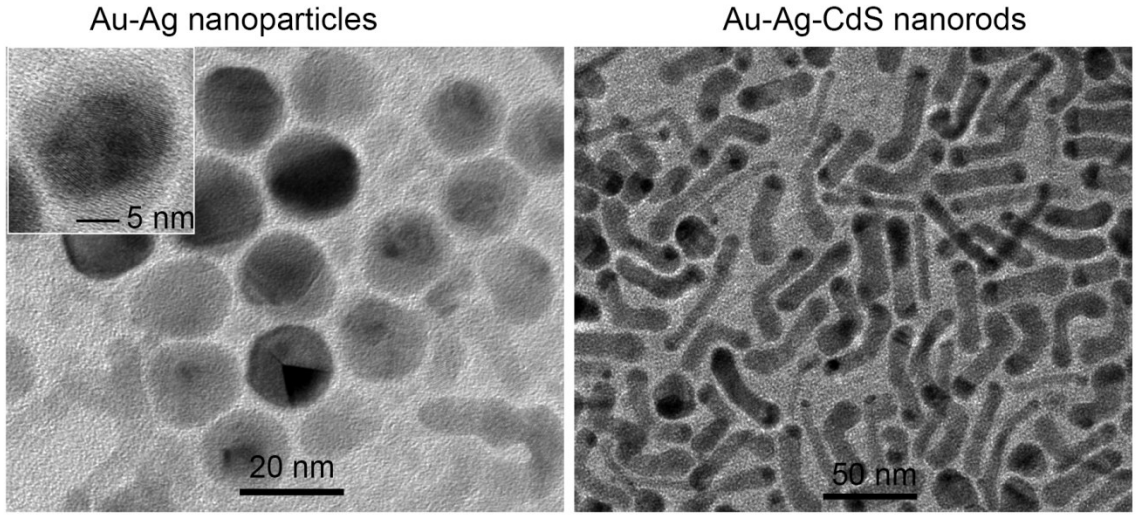

Figure S12. TEM images of Au-Ag nanoparticles, and Au-Ag-CdS hybrid nanorods. The inset is HRTEM image of Au-Ag nanoparticles. The same reaction scale and conditions were employed as described in the Ag based-CdS reactions. The only difference was that Au-Ag seeds were used instead of Ag seeds.

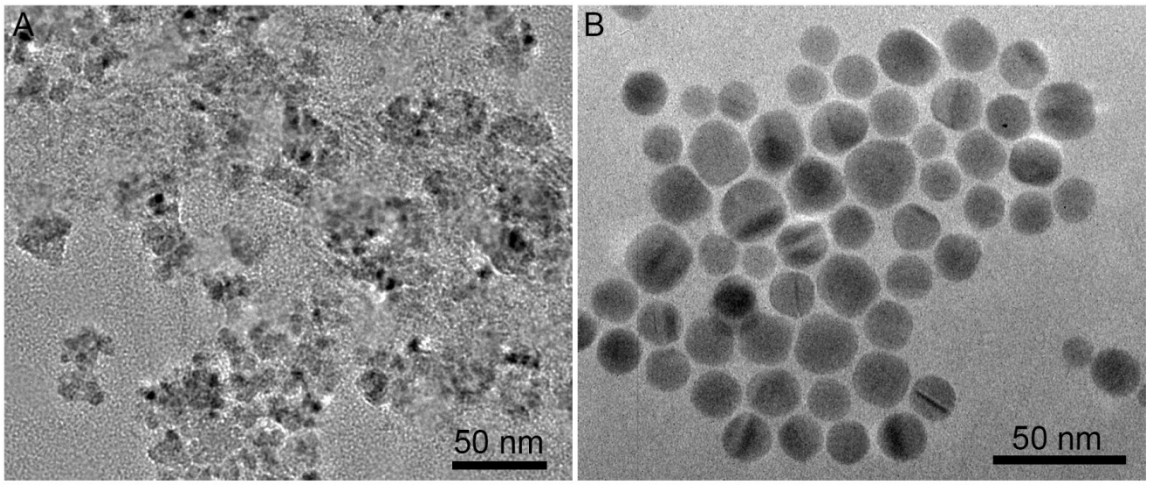

Figure S13. TEM images of irregular MnS nanoparticles, and spherical CdSe nanoparticles prepared without using Ag seeds.

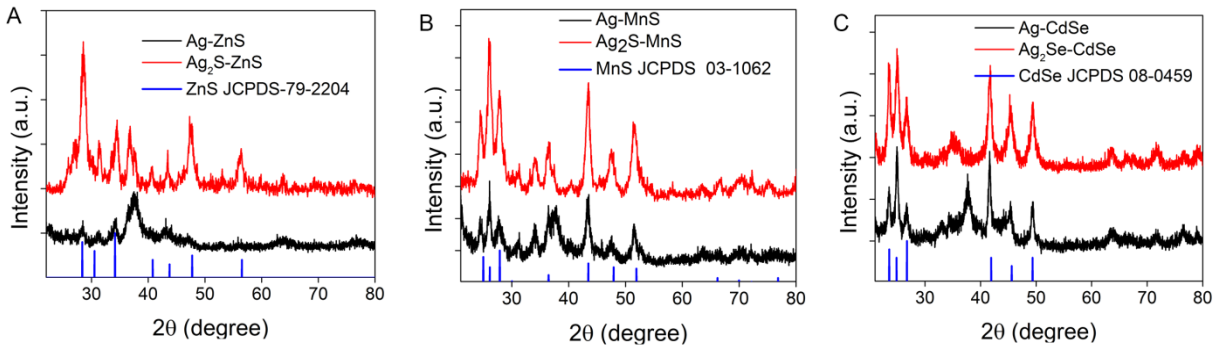

Figure S14. XRD patterns of (A) Ag-ZnS and Ag_2S-ZnS nanorods, (B) Ag-MnS and Ag_2S-MnS nanorods, and (C) Ag-CdSe and Ag_2Se-CdSe nanorods.

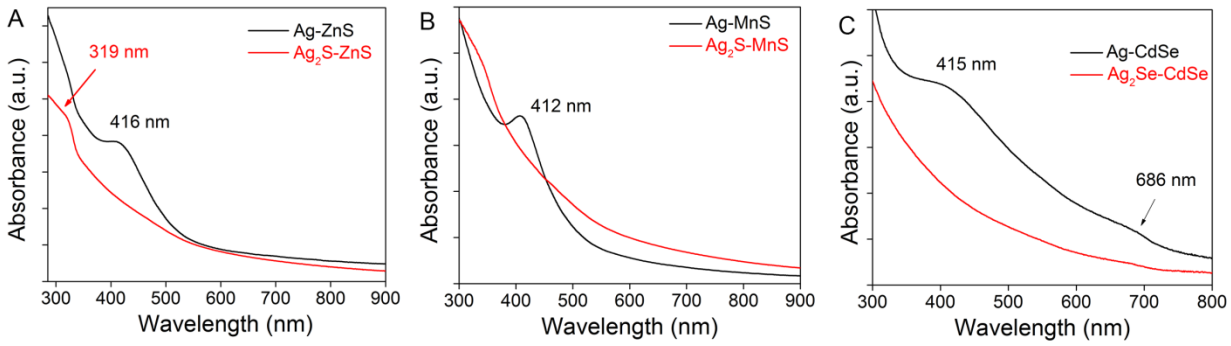

Figure S15. UV-Vis spectra of (A) Ag-ZnS and Ag_2S-ZnS nanorods, (B) Ag-MnS and Ag_2S-MnS nanorods, and (C) Ag-CdSe and Ag_2Se-CdSe nanorods.

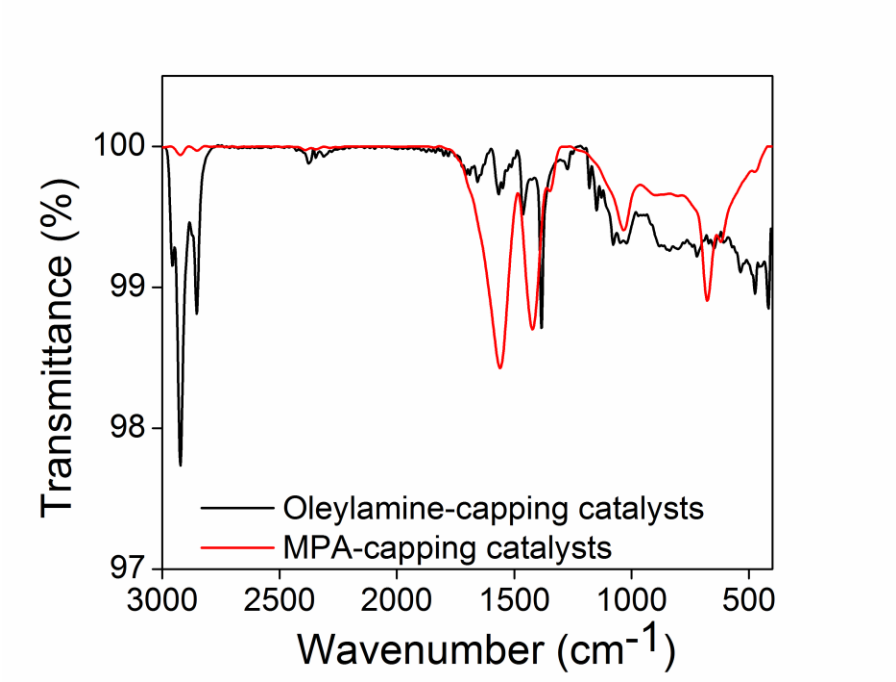

Figure S16. FT-IR spectra of different ligand- capped Ag-CdS nanorods. MPA: mercaptoproponic acid.

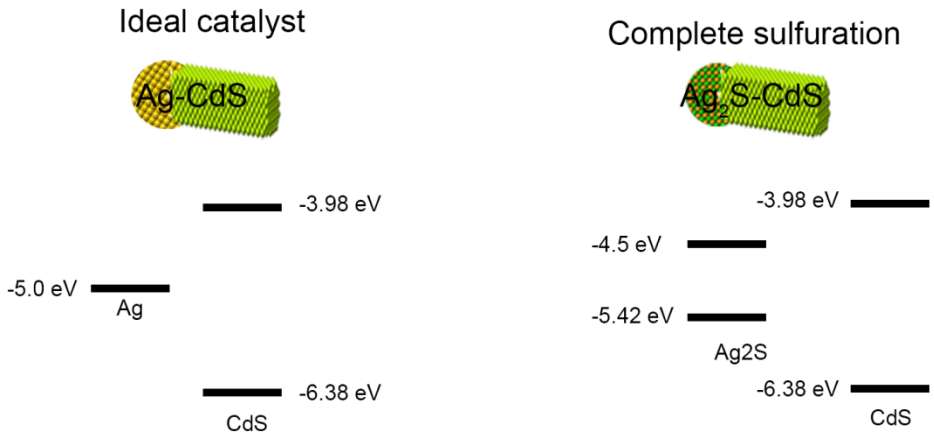

Figure S17. The energy band alignment of Ag and Ag_2S based CdS.